European Conference on Computational Fluid Dynamics
ECCOMAS CFD 2006
P. Wesseling, E. Oñate and J. Périaux (Eds)

THE ARTIFICIAL ADDED MASS EFFECT IN SEQUENTIAL STAGGERED FLUID-STRUCTURE INTERACTION ALGORITHMS

Christiane Förster*, Wolfgang A. Wall†, Ekkehard Ramm*

*University of Stuttgart, Institute of Structural Mechanics
Pfaffenwaldring 7, 70569 Stuttgart, Germany
e-mail: {foerster/ramm}@ibb.uni-stuttgart.de
web page: http://www.ibb.uni-stuttgart.de/members/{foerster/ramm}
†Technical University of Munich, Chair of Computational Mechanics,
Boltzmannstraße 15, 85747 Garching b. München, Germany
e-mail: wall@lnm.mw.tum.de

Key words: Fluid-structure interaction, Artificial added mass, Partitioned procedures, Coupled problems

Abstract. *The artificial added mass effect inherent in sequentially staggered coupling schemes is investigated by means of a fluid-structure interaction problem. A discrete representation of a simplified added mass operator in terms of the participating coefficient matrices is given and 'instability conditions' are evaluated for different temporal discretisation schemes.*

With respect to the time discretisation two different cases are distinguished. Discretisation schemes with stationary characteristics might allow for stable computations when good natured problems are considered. Such schemes yield a constant instability limit. Temporal discretisation schemes which exhibit recursive characteristics however yield an instability condition which is increasingly restrictive with every further step. Such schemes will therefore definitively fail in long time simulations irrespective of the problem parameters. It is also shown that for any sequentially staggered scheme and given spatial discretisation of a problem, a mass ratio between fluid and structural mass density exists at which the coupled system becomes unstable.

Numerical observations confirm the theoretical results.

1 INTRODUCTION

Partitioned algorithms are an appropriate way to deal with surface coupled problems such as fluid-structure interaction. Specificly designed solution schemes can be employed on the single fields and existing codes can conveniently be coupled. A particularly appealing way to solve the above coupled problem is a sequentially staggered formulation. While the fluid and structural domains are solved implicitly the coupling information (4)

and (5) is exchanged once per time step which introduces explicit features. However sequentially staggered schemes exhibit an inherent instability when used on fluid-structure interaction problems where incompressible flows are considered. The instability can be overcome by iteratively staggered partitioned schemes also called strongly coupled which utilise subiterations over the single fields to converge to the solution of the monolithic system.

The present work further clarifies the destabilising property of the so-called added mass effect[1,2] on sequentially staggered fluid structure calculations. It has been observed that loose coupling of fluid and structural part in the context of incompressible flow and slender structures frequently yields unstable computations. Surprisingly the instability depends upon the densities of fluid and structure and also on the geometry of the domain[1,2,3]. Clearly sequential coupling introduces an explicit flavour into the computation even if both partitions themselves are solved implicitly. Thus restrictions on the time step have to be expected. Observations however show that decreasing of the time step results in an increased instability. The instability is inherent in the scheme itself and has been named 'artificial added mass effect' since major parts of the fluid act as an extra mass on the structural degrees of freedom at the coupling interface. In sequentially staggered schemes the fluid forces depend upon predicted structural interface displacements rather than the correct ones and thus contain a portion of incorrect coupling forces. It is this 'artificial' contribution to the coupling which yields the instability.

The added mass effect has been investigated by means of a reduced model problem by Causin, Gerbeau and Nobile[3] where it is shown that the onset of the instability can be predicted well within the simplified problem. Here we wish to investigate the effect of these results on different time discretisation schemes and want to understand the influence of small time steps on the onset of the instability of sequentially staggered schemes.

A detailed analysis shows why more accurate schemes tend to be even more unstable. We employ generalised-α time integration on the structural part and consider backward Euler, the trapezoidal rule and second order backward differencing (BDF2) on the fluid domain. Further different predictors and ways to obtain the Dirichlet boundary condition on the fluid partition along the coupling interface are used.

We also show that every sequentially staggered scheme for incompressible flow will get unstable provided that the mass density ratio of fluid and structure is high enough. These results are confirmed by numerical observations.

2 STATEMENT OF THE PROBLEM

2.1 Governing equations

We consider problems consisting of a fluid (occupying Ω^F) and a structural part (in Ω^S) which interact at the common boundary Γ. This interface Γ is represented by a line or a curved surface in two- or three-dimensional problems, respectively. The possibly large

motion of the structure is governed by

$$\rho^S \frac{D^2\mathbf{d}}{Dt^2} - \boldsymbol{\nabla} \cdot (\boldsymbol{F} \cdot \boldsymbol{S}(\mathbf{d})) = \rho^S \mathbf{b}^S \qquad \text{in } \Omega^S \times (0,T), \tag{1}$$

where $\mathbf{d}$ represents the structural displacement and $\mathbf{b}^S$ body forces applied on the structure. The second order tensor $\boldsymbol{S}$ denotes the second Piola-Kirchhoff stress tensor and depends upon the particular material of the structure while $\boldsymbol{F}$ represents the deformation gradient tensor. Within the numerical investigations reported here linear St.-Venant-Kirchhoff material has been employed. The structural density is given by ρ^S. Either Neumann or Dirichlet boundary conditions apply at the not wetted part of the structural boundary $\partial\Omega^S \setminus \Gamma$.

The considered Newtonian fluid is governed by the incompressible Navier-Stokes equations

$$\rho^F \left.\frac{d\mathbf{u}}{dt}\right|_{\boldsymbol{\chi}} + \rho^F \left(\mathbf{u} - \mathbf{u}^G\right) \cdot \boldsymbol{\nabla}\mathbf{u} - 2\mu \boldsymbol{\nabla} \cdot \boldsymbol{\varepsilon}(\mathbf{u}) + \boldsymbol{\nabla}\bar{p} = \rho^F \mathbf{b}^F \qquad \text{in } \Omega^F \times (0,T), \tag{2}$$

$$\boldsymbol{\nabla} \cdot \mathbf{u} = 0 \qquad \text{in } \Omega^F \times (0,T). \tag{3}$$

Here $\mathbf{u}$ denotes the fluid velocity field and $\bar{p}$ the physical pressure. The fluid density and viscosity are given by ρ^F and μ, respectively. The vector $\mathbf{b}^F$ represents fluid body forces and $\boldsymbol{\varepsilon}(\mathbf{u}) = \frac{1}{2}\left(\boldsymbol{\nabla}\mathbf{u} + (\boldsymbol{\nabla}\mathbf{u})^T\right)$ denotes the strain rate tensor.

Suitable (Dirichlet or Neumann) boundary conditions apply at the boundary of the fluid domain which is not coupled to the structure $\partial\Omega^F \setminus \Gamma$.

At the FSI interface Γ kinematic and dynamic continuity is required. As in viscous flows the fluid particles stick to the structure at the common interface, a local Lagrangian formulation at Γ can be assumed. Thus denoting the material time derivative by an over-set dot the kinematic coupling conditions read

$$\mathbf{d}_\Gamma(t) = \mathbf{r}_\Gamma^F(t), \qquad \dot{\mathbf{d}}_\Gamma(t) = \mathbf{u}_\Gamma(t) = \dot{\mathbf{x}}_\Gamma^F(t), \qquad \ddot{\mathbf{d}}_\Gamma(t) = \dot{\mathbf{u}}_\Gamma(t). \tag{4}$$

Here $\mathbf{r}_\Gamma^F(t)$ represents the displacement of the fluid interface. The dynamic coupling condition demands the equilibrium of the traction at Γ

$$\mathbf{h}^S(t) + \mathbf{h}^F(t) = \mathbf{0} \tag{5}$$

where $\mathbf{h} = \boldsymbol{\sigma} \cdot \mathbf{n}$ denotes the traction vector on either field which is obtained from the Cauchy stress tensor.

2.2 Sequentially staggered algorithm

The class of algorithms considered here is outlined in the following. After independent temporal discretisation of both fields by means of finite differences the time step from time level n to $n+1$ proceeds as follows where we assume the same time step size Δt on both fields for brevity:

(a) Calculate an explicit predictor of the structural interface displacement at the new time level $\mathbf{d}_{\Gamma,P}^{n+1}$.

(b) Compute fluid velocity at Γ to serve as Dirichlet boundary condition $\mathbf{u}_{\Gamma,P}^{n+1}\left(\mathbf{d}_{\Gamma,P}^{n+1}\right)$.

(c) Update the mesh displacement $\mathbf{r}^{n+1}\left(\mathbf{d}_{\Gamma,P}^{n+1}\right)$.

(d) Solve fluid equations on the deforming domain to obtain $\mathbf{u}^{n+1}$ and $\bar{p}^{n+1}$.

(e) Obtain fluid boundary traction along Γ $\mathbf{h}_{\Gamma}^{F,n+1}$.

(f) Solve the structural field for the new displacements $\mathbf{d}^{n+1}$ under consideration of the fluid load $\mathbf{h}_{\Gamma}^{F,n+1}$.

(g) Proceed to next time step.

To further specify the above algorithm the single discretisation schemes have to be stated.

The time discretisation of the structural problem is performed by means of a nonlinear version of the generalised-α time integration scheme of Chung and Hulbert[4] which is based on the Newmark scheme

$$\mathbf{d}^{n+1} = \mathbf{d}^{n} + \Delta t \dot{\mathbf{d}}^{n} + \Delta t^2 \left(\left(\frac{1}{2} - \beta \right) \ddot{\mathbf{d}}^{n} + \beta \ddot{\mathbf{d}}^{n+1} \right) \tag{6}$$

$$\dot{\mathbf{d}}^{n+1} = \dot{\mathbf{d}}^{n} + \Delta t \left((1-\gamma) \ddot{\mathbf{d}}^{n} + \gamma \ddot{\mathbf{d}}^{n+1} \right) \tag{7}$$

The generalised-α scheme satisfies the equilibrium of linear momentum at an intermediate time level t^{α} between t^{n} and t^{n+1}

$$\rho^{S} \ddot{\mathbf{d}}^{\alpha} - \boldsymbol{\nabla} \cdot (\boldsymbol{F} \cdot \boldsymbol{S}(\mathbf{d}^{\alpha})) = \mathbf{0},$$

where zero body forces are assumed for brevity. Displacements, velocities and accelerations of the structure are interpolated between the discrete time levels by

$$\ddot{\mathbf{d}}^{\alpha} = (1-\alpha_m)\ddot{\mathbf{d}}^{n+1} + \alpha_m \ddot{\mathbf{d}}^{n}, \tag{8}$$

$$\dot{\mathbf{d}}^{\alpha} = (1-\alpha_f)\dot{\mathbf{d}}^{n+1} + \alpha_f \dot{\mathbf{d}}^{n}, \tag{9}$$

$$\mathbf{d}^{\alpha} = (1-\alpha_f)\mathbf{d}^{n+1} + \alpha_f \mathbf{d}^{n}. \tag{10}$$

The integration constants are chosen such that the overall scheme has the desired spectral radius ρ_{∞} while also minimal damping on low frequency modes is ensured. Evaluating α_m, α_f, β and γ from

$$\alpha_m = \frac{2\rho_{\infty} - 1}{\rho_{\infty} + 1}, \qquad \alpha_f = \frac{\rho_{\infty}}{\rho_{\infty} + 1}$$

$$\alpha_m \leq \alpha_f \leq \frac{1}{2}, \qquad \beta = \frac{1}{4}\left(1 - \alpha_m + \alpha_f\right)^2, \qquad \gamma = \frac{1}{2} - \alpha_m + \alpha_f$$

yields a second order accurate system.

Temporal discretisation of the fluid equations is performed by means of different schemes. The simplest implicit scheme is backward Euler (BE) which is just first order accurate.

$$\frac{\mathbf{u}^{n+1} - \mathbf{u}^n}{\Delta t} = \dot{\mathbf{u}}^{n+1}. \tag{11}$$

Further the trapezoidal rule (TR)

$$\frac{\mathbf{u}^{n+1} - \mathbf{u}^n}{\Delta t} = \frac{1}{2}\,\dot{\mathbf{u}}^{n+1} + \frac{1}{2}\,\dot{\mathbf{u}}^n \tag{12}$$

and second order backward differencing (BDF2)

$$\frac{\mathbf{u}^{n+1} - \mathbf{u}^n}{\Delta t} = \frac{1}{3}\,\frac{\mathbf{u}^n - \mathbf{u}^{n-1}}{\Delta t} + \frac{2}{3}\,\dot{\mathbf{u}}^{n+1} \tag{13}$$

are considered.

The structural predictor is another important ingredient which influences the onset of the instabilities observed. Following Mok[1] three different predictors of differing order of accuracy shall be considered here. A simple predictor which is zeroth order in time is given by

$$\mathbf{d}_{\Gamma,P}^{n+1} = \mathbf{d}_{\Gamma}^{n}. \tag{14}$$

As a first order predictor

$$\mathbf{d}_{\Gamma,P}^{n+1} = \mathbf{d}_{\Gamma}^{n} + \Delta t \dot{\mathbf{d}}_{\Gamma}^{n} \tag{15}$$

is used while

$$\mathbf{d}_{\Gamma,P}^{n+1} = \mathbf{d}_{\Gamma}^{n} + \Delta t \left(\frac{3}{2}\dot{\mathbf{d}}_{\Gamma}^{n} - \frac{1}{2}\dot{\mathbf{d}}_{\Gamma}^{n-1} \right) \tag{16}$$

is a second order accurate predicted interface displacement.

The boundary condition applied to the fluid at the boundary Γ is also required to fully specify the temporally discretised scheme. A first order interpolation yields

$$\mathbf{u}_{\Gamma}^{n+1} = \frac{\mathbf{d}_{\Gamma,P}^{n+1} - \mathbf{d}_{\Gamma,P}^{n}}{\Delta t}. \tag{17}$$

Equation (17) is a backward Euler discretisation of the fluid velocity at the coupling interface Γ. Accurate conservation of the size of the fluid domain Ω^F requires to employ a second order discretisation of the fluid boundary velocity $\mathbf{u}_{\Gamma} = \dot{\mathbf{d}}$ in time yielding

$$\mathbf{u}_{\Gamma}^{n+1} = 2\,\frac{\mathbf{d}_{\Gamma,P}^{n+1} - \mathbf{d}_{\Gamma,P}^{n}}{\Delta t} - \mathbf{u}_{\Gamma}^{n}. \tag{18}$$

Equation (18) uses the trapezoidal rule and ensures that the discrete velocity function integrates in time to the discrete locations of the interface. Despite this desirable property (18) exhibits the tendency of the trapezoidal rule to oscillations and can thus not generally be recommended.

2.3 Observed Instability

Sequentially staggered schemes coupling structures and incompressible fluids exhibit an inherent instability which increases with decreasing time step. This problem has been described by Mok[1,2] and its mathematical background has recently been provided by Causin et al.[3]. The following observations have been made:

- With decreasing Δt the instability occurs earlier.
- The mass ratio between fluid and structure has a significant influence on the stability of the staggered system. The bigger the mass ratio $\frac{\rho^F}{\rho^S}$ the worse the instability gets.
- Numerical observations indicate that increased fluid viscosity increases the instability while increased structural stiffness offers a light decreasing effect.
- The actual onset of unconditional instability depends upon the particular combination of temporal discretisation items.

Especially the first point indicates that the instability is not due to a too large time step size. It is rather caused by too large eigenvalues of the amplification operator of the explicit step.

3 DERIVATION OF THE ADDED MASS OPERATOR

3.1 Discretisation in space

The fluid equations (2) and (3) are discretised in space by means of finite elements. The spatial domain Ω^F is divided into non-overlapping patches, the elements. The spatial discretisation maintains its topology while following the deformation of the domain. Within the present investigation of the instability due to the sequentially staggered coupling scheme the motion of the domain is a secondary matter and not taken into account subsequently.

To define the Galerkin weak form we select C^0 Lagrangian finite element spaces $\mathbf{V}_0^h \subset \mathbf{H}_0^1(\Omega^F)$ and $\mathbf{V}^h \subset \mathbf{H}^1(\Omega^F)$, where $\mathbf{V}^h$ satisfies the time dependent Dirichlet boundary conditions of the problem while all functions in $\mathbf{V}_0^h$ are zero on Γ_D^F. The pressure is taken from the space $P^h \subset L^2(\Omega^F)$ of square integrable functions.

The discrete variational statement is as follows: seek $\mathbf{u} \in \mathbf{V}^h$, $p \in P^h$ such that

$$B\left(\{\mathbf{u}, p\}, \{\mathbf{v}, q\}\right) = \left(\mathbf{f}^F, \mathbf{v}\right) + \left(\mathbf{h}^F, \mathbf{v}\right)_{\Gamma_N^F} \qquad \forall\, (\mathbf{v}, q) \in (\mathbf{V}_0^h, P^h), \tag{19}$$

where the discrete operator $B\left(\{\mathbf{u},p\},\{\mathbf{v},q\}\right)$ is given by

$$\begin{aligned} B\left(\{\mathbf{u},p\},\{\mathbf{v},q\}\right) = (\dot{\mathbf{u}},\mathbf{v}) + \left((\mathbf{u}-\mathbf{u}^G)\cdot\boldsymbol{\nabla}\mathbf{u},\mathbf{v}\right) + (2\nu\boldsymbol{\varepsilon}(\mathbf{u}),\boldsymbol{\varepsilon}(\mathbf{v})) \\ - (p,\boldsymbol{\nabla}\cdot\mathbf{v}) - (q,\boldsymbol{\nabla}\cdot\mathbf{u})\,. \end{aligned} \tag{20}$$

Here $(\cdot,\cdot)$ denotes the L^2 inner product on the fluid domain Ω^F and $\nu = \frac{\mu}{\rho^F}$ the kinematic viscosity.

The spatially discretised equations are conveniently expressed in matrix notation

$$\begin{aligned} \mathbf{M}^F\dot{\mathbf{u}} + \mathbf{K}^F\mathbf{u} + \mathbf{G}\mathbf{p} &= \mathbf{f}_\Gamma \\ \mathbf{G}^T\mathbf{u} &= \mathbf{0}, \end{aligned} \tag{21}$$

where $\mathbf{M}^S$ and $\mathbf{K}^S$ denote the mass and 'stiffness' of the fluid while $\mathbf{G}$ is the discrete gradient operator on the pressure field. The vectors $\mathbf{u}$ and $\mathbf{p}$ contain the nodal velocity and pressure values, respectively. In (21) the right hand side is built by contributions from fluid structure interaction only.

Discretisation of the structural equation (1) yields

$$\mathbf{M}^S\ddot{\mathbf{d}} + \mathbf{K}^S\mathbf{d} = -\mathbf{f}_\Gamma, \tag{22}$$

where $\mathbf{M}^S$ and $\mathbf{K}^S$ denote the mass and stiffness matrix of the structure, respectively, and $\mathbf{d}$ is the vector of nodal displacements. The right hand side consists of contributions at the interface nodes which is the discrete representation of the traction in equation (5).

3.2 Spatially discrete representation of the added mass operator

In order to work out the instability of the staggered coupled system the spatially discretised representations of the field equations (1) to (3) are employed. Further some simplifications are made to ease the analysis.

- The discretisation of fluid and structure is conforming along the interface Γ.
- Both field equations can be regarded as linear or have been linearised.
- The influence of mesh motion and thus the temporal change of all significant matrices is negligible.
- The structural density ρ^S remains constant.
- There are no external forces except the traction along Γ.
- There is no physical structural damping assumed.

The first assumption simply eases the presentation while the other assumptions are reasonable as the instability we consider typically occurs at very early time steps i.e. when no significant nonlinearity has been built up.

To further simplify the analysis the fluid stiffness is omitted in (21) at this point. This is reasonable as the instabilities we consider increase with decreasing time step. After time discretisation the discrete equations will be dominated by the mass and pressure terms when very small time steps are employed. Thus, this simplification allows to clearly highlight the reason of the instability. The simplified fluid system of equations is now split up into degrees of freedom belonging to the interior of the fluid domain and others at the interface. The assumption that the coefficient matrices do not change in time allows to use the ALE time derivative of the divergence equation

$$\left.\frac{\partial\left(\mathbf{G}^T\mathbf{u}\right)}{\partial t}\right|_{\chi} = \overset{\cdot}{\overline{\mathbf{G}^T\mathbf{u}}} = \mathbf{G}^T\dot{\mathbf{u}} \tag{23}$$

and thus

$$\begin{bmatrix} \mathbf{M}^F_{II} & \mathbf{M}^F_{I\Gamma} & \mathbf{G}_I \\ \mathbf{M}^F_{\Gamma I} & \mathbf{M}^F_{\Gamma\Gamma} & \mathbf{G}_\Gamma \\ \mathbf{G}_I^T & \mathbf{G}_\Gamma^T & \mathbf{0} \end{bmatrix} \begin{bmatrix} \dot{\mathbf{u}}_I \\ \dot{\mathbf{u}}_\Gamma \\ \mathbf{p} \end{bmatrix} = \begin{bmatrix} \mathbf{0} \\ \mathbf{f}_\Gamma \\ \mathbf{0} \end{bmatrix}. \tag{24}$$

Using the prescribed interface acceleration obtained from the structural prediction, the system (24) yields the solution vectors

$$\mathbf{p} = \left(\mathbf{G}_I^T\left(\mathbf{M}^F_{II}\right)^{-1}\mathbf{G}_I\right)^{-1}\left\{-\mathbf{G}_I^T\left(\mathbf{M}^F_{II}\right)^{-1}\mathbf{M}^F_{I\Gamma} + \mathbf{G}_\Gamma^T\right\}\dot{\mathbf{u}}_\Gamma, \tag{25}$$

$$\dot{\mathbf{u}}_I = -\left(\mathbf{M}^F_{II}\right)^{-1}\mathbf{M}^F_{I\Gamma}\,\dot{\mathbf{u}}_\Gamma + \left(\mathbf{M}^F_{II}\right)^{-1}\mathbf{G}_I\left(\mathbf{G}_I^T\left(\mathbf{M}^F_{II}\right)^{-1}\mathbf{G}_I\right)^{-1}\left\{\mathbf{G}_I^T\left(\mathbf{M}^F_{II}\right)^{-1}\mathbf{M}^F_{I\Gamma} - \mathbf{G}_\Gamma^T\right\}\dot{\mathbf{u}}_\Gamma. \tag{26}$$

Employing the second line of the system (24) the interfacial coupling force $\mathbf{f}_\Gamma$ can now be expressed in terms of the interface acceleration.

$$\begin{aligned}\mathbf{f}_\Gamma = \Bigg\{&\left(\mathbf{M}^F_{\Gamma I}\left(\mathbf{M}^F_{II}\right)^{-1}\mathbf{G}_I - \mathbf{G}_\Gamma\right)\left(\mathbf{G}_I^T\left(\mathbf{M}^F_{II}\right)^{-1}\mathbf{G}_I\right)^{-1}\left(\mathbf{G}_I^T\left(\mathbf{M}^F_{II}\right)^{-1}\mathbf{M}^F_{I\Gamma} - \mathbf{G}_\Gamma^T\right)\\ &- \mathbf{M}^F_{\Gamma I}\left(\mathbf{M}^F_{II}\right)^{-1}\mathbf{M}^F_{I\Gamma} + \mathbf{M}^F_{\Gamma\Gamma}\Bigg\}\,\dot{\mathbf{u}}_\Gamma\end{aligned} \tag{27}$$

The discrete operator in curly brackets has the dimension of a mass. It can be normalised by a characteristic fluid mass m^F (which is for example a nodal mass of a lumped mass matrix) to recover a discrete representation of the added mass operator.

$$\begin{aligned}\boldsymbol{\mathcal{M}}_{\boldsymbol{\mathcal{A}}} := &\frac{1}{m^F}\left(\mathbf{M}^F_{\Gamma I}\left(\mathbf{M}^F_{II}\right)^{-1}\mathbf{G}_I - \mathbf{G}_\Gamma\right)\left(\mathbf{G}_I^T\left(\mathbf{M}^F_{II}\right)^{-1}\mathbf{G}_I\right)^{-1}\left(\mathbf{G}_I^T\left(\mathbf{M}^F_{II}\right)^{-1}\mathbf{M}^F_{I\Gamma} - \mathbf{G}_\Gamma^T\right)\\ &- \frac{1}{m^F}\mathbf{M}^F_{\Gamma I}\left(\mathbf{M}^F_{II}\right)^{-1}\mathbf{M}^F_{I\Gamma} + \frac{1}{m^F}\mathbf{M}^F_{\Gamma\Gamma}\end{aligned} \tag{28}$$

Employing the added mass operator (28) yields the fluid forces at the coupling boundary

$$\mathbf{f}_\Gamma = m^F \boldsymbol{\mathcal{M}}_{\boldsymbol{\mathcal{A}}} \dot{\mathbf{u}}_\Gamma. \tag{29}$$

The added mass operator $\boldsymbol{\mathcal{M}}_{\boldsymbol{\mathcal{A}}}$ contains the condensed fluid equations and maps a dimensionless interface acceleration onto an also dimensionless force vector at the interface Γ. Thus the operator is purely geometrical. It can be observed from (28) that the discrete added mass operator is symmetric and positive.

A further interesting simplification is to use a lumped fluid mass matrix which yields the simple expression

$$\boldsymbol{\mathcal{M}}_{\boldsymbol{\mathcal{A}}l} = \mathbf{I}^F_{\Gamma\Gamma} + 2\,\mathbf{G}_\Gamma \left(\mathbf{G}_I^T \mathbf{G}_I\right)^{-1} \mathbf{G}_\Gamma^T \tag{30}$$

for the lumped added mass operator. In (30) a regular mesh is assumed. Thus the nodal mass of an interior node is twice as big as the mass of a coupled node which has half the support of the former.

4 STABILITY OF THE SEQUENTIALLY COUPLED PROBLEM

Introducing the coupling force (29) into the discrete linearised structural equation (22) yields

$$\begin{bmatrix} \mathbf{M}^S_{II} & \mathbf{M}^S_{I\Gamma} \\ \mathbf{M}^S_{\Gamma I} & \mathbf{M}^S_{\Gamma\Gamma} \end{bmatrix} \begin{bmatrix} \ddot{\mathbf{d}}_I \\ \ddot{\mathbf{d}}_\Gamma \end{bmatrix} + \begin{bmatrix} \mathbf{K}^S_{II} & \mathbf{K}^S_{I\Gamma} \\ \mathbf{K}^S_{\Gamma I} & \mathbf{K}^S_{\Gamma\Gamma} \end{bmatrix} \begin{bmatrix} \mathbf{d}_I \\ \mathbf{d}_\Gamma \end{bmatrix} = \begin{bmatrix} \mathbf{0} \\ -m^F \boldsymbol{\mathcal{M}}_{\boldsymbol{\mathcal{A}}}\, \dot{\mathbf{u}}_\Gamma \end{bmatrix}, \tag{31}$$

where within the staggered scheme the fluid interface acceleration $\dot{\mathbf{u}}_\Gamma$ is obtained from a structural prediction of the new interface displacement.

Equation (31) reveals why $\boldsymbol{\mathcal{M}}_{\boldsymbol{\mathcal{A}}}$ is named 'added mass operator'. Identifying the fluid interface acceleration $\dot{\mathbf{u}}_\Gamma$ with the structural interface acceleration $\ddot{\mathbf{d}}_\Gamma$ shows that the product $m^F \boldsymbol{\mathcal{M}}_{\boldsymbol{\mathcal{A}}}$ works as an additional mass on the interface degrees of freedom.

4.1 Schemes with stationary characteristics

The stability or instability of the scheme (31) solved in an sequentially staggered manner depends upon the particular time discretisation employed. The most stable version of the structural generalised-α time discretisation scheme is obtained when maximal numerical dissipation is involved i.e. when the spectral radius of the scheme is set to $\rho_\infty = 0.0$. This yields the parameter $\alpha_m = -1$, $\alpha_f = 0$, $\beta = 1$ and $\gamma = \frac{3}{2}$. By means of (6) to (8) an expression for the structural acceleration in terms of displacements can be obtained

$$\ddot{\mathbf{d}}^\alpha = \frac{1}{\Delta t^2} \left(2\mathbf{d}^{n+1} - 5\mathbf{d}^n + 4\mathbf{d}^{n-1} - \mathbf{d}^{n-2}\right). \tag{32}$$

The fluid acceleration $\dot{\mathbf{u}}_\Gamma$ is also expressed in terms of structural displacements. Using backward Euler time integration (12), the zeroth order interface predictor (14) and the

first order interpolation of the boundary condition at the interface yields

$$\dot{\mathbf{u}}_\Gamma^{n+1} = \frac{1}{\Delta t^2}\left(\mathbf{d}_\Gamma^n - 2\mathbf{d}_\Gamma^{n-1} + \mathbf{d}_\Gamma^{n-2}\right). \tag{33}$$

Inserting (32) into the discrete linearised structural system of equations gives

$$\mathbf{M}^S \frac{1}{\Delta t^2}\left(2\mathbf{d}^{n+1} - 5\mathbf{d}^n + 4\mathbf{d}^{n-1} - \mathbf{d}^{n-2}\right) + \mathbf{K}^S\mathbf{d}^{n+1} = \mathbf{f}^{n+1}, \tag{34}$$

where $\mathbf{f}^{n+1}$ represents all types of forces on the structure at the new time level $n+1$. For very small time steps (34) is dominated by the mass term while the stiffness looses influence. Omitting the stiffness and lumping the mass term in a temporally discretised version of (31) allows to reduce the system to the interfacial degrees of freedom

$$m^S\left(2\mathbf{d}^{n+1} - 5\mathbf{d}^n + 4\mathbf{d}^{n-1} - \mathbf{d}^{n-2}\right) + m^F\boldsymbol{\mathcal{M}}_{\boldsymbol{\mathcal{A}}}\left(\mathbf{d}_\Gamma^n - 2\mathbf{d}_\Gamma^{n-1} + \mathbf{d}_\Gamma^{n-2}\right) = \mathbf{0}. \tag{35}$$

As the added mass operator $\boldsymbol{\mathcal{M}}_{\boldsymbol{\mathcal{A}}}$ is a real positive matrix all vectors in (35) can be expanded in terms of the eigenvectors $\mathbf{v}_i$ of $\boldsymbol{\mathcal{M}}_{\boldsymbol{\mathcal{A}}}$ i.e. $\mathbf{d}_\Gamma = \sum_i d_i\mathbf{v}_i$. The scalar coefficients d_i have to satisfy

$$2d_i^{n+1} - 5d_i^n + 4d_i^{n-1} - d_i^{n-2} + \mu_i\frac{m^F}{m^S}\left(d_i^n - 2d_i^{n-1} + d_i^{n-2}\right) = 0, \tag{36}$$

where μ_i represents the ith eigenvalue of $\boldsymbol{\mathcal{M}}_{\boldsymbol{\mathcal{A}}}$. Inserting the amplification factor λ_i with $d_i^{n+1} = \lambda_i d_i^n$ into (36) yields the characteristic polynomial of (36) associated with μ_i.

$$2\lambda_i^3 - 5\lambda_i^2 + 4\lambda_i - 1 + \mu_i\frac{m^F}{m^S}\left(\lambda_i^2 - 2\lambda_i + 1\right) = p(\lambda_i) = 0 \tag{37}$$

All solutions λ_i of (37) have to satisfy $|\lambda_i| \leq 1$ if the scheme (35) is stable. As $p(-\infty) = -\infty$ and $p(-1) = -12 + 4\,\frac{m^F}{m^S}\,\mu_i$ there exists a solution $p(\lambda^*) = 0$ with $\lambda^* < -1$ as soon as

$$\frac{m^F}{m^S}\max_i \mu_i > 3, \tag{38}$$

which is thus an instability condition, i.e. the sequentially staggered system is unstable if (38) is satisfied.

As all the ingredients of the above scheme are very good-natured in the sense that high numerical damping on both the structural and fluid part is involved, (38) is a very permissive result. Repeating the analysis by using BDF2 (13) rather than BE to discretise the fluid part in time yields

$$\dot{\mathbf{u}}_\Gamma^{n+1} = \frac{1}{2\,\Delta t^2}\left(3\mathbf{d}_\Gamma^n - 7\mathbf{d}_\Gamma^{n-1} + 5\mathbf{d}_\Gamma^{n-2} - \mathbf{d}_\Gamma^{n-3}\right). \tag{39}$$

In this case the characteristic polynomial is given by

$$4\lambda_i^4 - 10\lambda_i^3 + 8\lambda_i^2 - 2\lambda_i + \mu_i \frac{m^F}{m^S}\left(3\lambda_i^3 - 7\lambda_i^2 + 5\lambda_i - 1\right) = p(\lambda_i) = 0 \tag{40}$$

and yields the instability condition

$$\frac{m^F}{m^S}\max_i \mu_i > \frac{3}{2}. \tag{41}$$

Changing from first order accurate BE to BDF2 on the fluid part of the problem results in an instability condition which is twice as restrictive. Table 1 summarises the instability constants C_{inst} of the instability condition

$$\frac{m^F}{m^S}\max_i \mu_i > C_{inst} \tag{42}$$

obtained with generalised-α time integration (with $\rho_\infty = 0$) of the structural domain, first order interpolation at the interface Γ (17) and the different structural predictors (14)-(16).

predictor	BE	BDF2
0th order	3	$\frac{3}{2}$
1st order	$\frac{3}{5}$	$\frac{3}{10}$
2nd order	$\frac{1}{3}$	$\frac{1}{6}$

Table 1: Instability constant C_{inst} in condition (42) obtained for sequentially staggered fluid-structure interaction schemes depending upon the structural predictors (14)-(16) and the fluid time discretisation scheme

It shows that increased accuracy significantly increases the stability problems. Another remarkable result is that switching from BE to BDF2 on the fluid domain results in an instability condition twice as restrictive.

Clearly some of the combinations summarised here are not useful for practical computations as the overall order of temporal accuracy is governed by the lowest order ingredient. For the purpose of the present analysis however the effect of the single items is of interest. It can easily be observed that a combination of a number of higher order elements such as BDF2 time discretisation on the fluid domain, a second order structural predictor at the interface and a second order accurate interface boundary condition on the fluid domain yields an even earlier instability.

4.2 Schemes with instationary characteristics

Couple schemes which employ the TR (12) for fluid time integration or use the geometrically correct version for the Dirichlet boundary condition on the fluid structure

interface (18) are a little more difficult to treat than the previous ones. Such algorithms do not exhibit an expression for the predicted fluid interface acceleration in terms of a limited number of previous interface displacements comparable to (33) but rather require all previous interface positions to be considered i.e. cycle down to the initial conditions.

To sample the following scheme is considered:

- structure:
  - generalised-α with $\rho_\infty = 0$
- fluid:
  - time discretisation: TR (12)
  - predictor: zeroth order (14)
  - Dirichlet boundary condition: first order (17)

Here we wish to investigate the particular influence of the trapezoidal rule employed on the fluid domain. The results obtained for a fully second order scheme with TR and a second order accurate predictor and boundary condition are even more restrictive.

While the structural acceleration is given by the expression (32), the fluid acceleration is obtained from

$$\dot{\mathbf{u}}_\Gamma^{n+1} = \frac{1}{\Delta t}\left(2\mathbf{d}_\Gamma^n - 4\mathbf{d}_\Gamma^n + 2\mathbf{d}_\Gamma^{n-1}\right) - \dot{\mathbf{u}}_\Gamma^n, \tag{43}$$

which cannot be expressed in interface displacements only. The amplification of the scheme thus depends upon the actual time step. Assuming that the initial condition includes zero acceleration of the interface i.e. $\dot{\mathbf{u}}_\Gamma^0 = \mathbf{0}$ the first step ($n = 0$) yields

$$2\mathbf{d}_\Gamma^1 - 5\mathbf{d}_\Gamma^0 + \boldsymbol{\mathcal{M}}_{\boldsymbol{\mathcal{A}}} \frac{m^F}{m^S} 2\mathbf{d}_\Gamma^0 = \mathbf{0} \tag{44}$$

and the characteristic polynomial

$$2\lambda - 5 + 2\mu_i \frac{m^F}{m^S} = p(\lambda) = 0. \tag{45}$$

With $p(\lambda = -\infty) = -\infty$ and $p(\lambda = -1) = -7 + 2\mu_i \frac{m^F}{m^S}$ one obtains the instability condition for the first step; the first step will be unstable if

$$\max_i \mu_i \frac{m^F}{m^S} > \frac{7}{2}. \tag{46}$$

With $n = 1$ we get

$$2\mathbf{d}_\Gamma^2 - 5\mathbf{d}_\Gamma^1 + 4\mathbf{d}_\Gamma^0 + \boldsymbol{\mathcal{M}}_{\boldsymbol{\mathcal{A}}} \frac{m^F}{m^S}\left(2\mathbf{d}_\Gamma^1 - 6\mathbf{d}_\Gamma^0\right) = \mathbf{0} \tag{47}$$

and

$$2\lambda^2 - 5\lambda + 4 + \mu_i \frac{m^F}{m^S}(2\lambda - 6) = p(\lambda) = 0. \tag{48}$$

As $p(\lambda = -\infty) = \infty$ and $p(\lambda = -1) = 11 - 8\mu_i \frac{m^F}{m^S}$ this yields the instability condition

$$\max_i \mu_i \frac{m^F}{m^S} > \frac{11}{8}. \tag{49}$$

Analogous the next ($n = 2$) step gives

$$2\mathbf{d}_\Gamma^3 - 5\mathbf{d}_\Gamma^2 + 4\mathbf{d}_\Gamma^1 - \mathbf{d}_\Gamma^0 + \boldsymbol{\mathcal{M}}_{\boldsymbol{\mathcal{A}}} \frac{m^F}{m^S}\left(2\mathbf{d}_\Gamma^2 - 6\mathbf{d}_\Gamma^1 + 8\mathbf{d}_\Gamma^0\right) = \mathbf{0}, \tag{50}$$

which by means of the characteristic polynomial

$$2\lambda^3 - 5\lambda^2 + 4\lambda - 1 + \mu_i \frac{m^F}{m^S}\left(2\lambda^2 - 6\lambda + 8\right) = p(\lambda) = 0. \tag{51}$$

yields the instability limit of the third step:

$$\max_i \mu_i \frac{m^F}{m^S} > \frac{3}{4}. \tag{52}$$

The instability conditions of all further steps n is obtained by simple calculation. It is given by

$$\max_i \mu_i \frac{m^F}{m^S} > \frac{12}{8\,n} \qquad \forall n > 1, \tag{53}$$

which shows that the scheme with fixed geometry and mass ratio becomes unstable after a limited number of steps irrespective of the mass ratio or the added mass operator themselves. Similar results can be obtained when the coupling condition (18) is employed. Additionally, the combination of higher order ingredients (time discretisation scheme, predictor, coupling condition) and a sub-cycling scheme destabilises even faster.

Thus a fluid time discretisation scheme which employs the trapezoidal rule (or also the one-step-θ scheme with $\theta \neq 1$) or the geometrically correct coupling condition (18) cannot be employed in a sequentially staggered scheme for stable long-time simulations.

4.3 General instability

Irrespective of the particular time discretisation schemes the sequential staggered coupling scheme itself carries an inherent instability as stated by the following theorem.

For every sequentially staggered scheme constructed as described in section 2.2, a mass ratio $\frac{m^F}{m^S}$ exists at which the overall algorithm becomes unstable.

For every sequentially staggered scheme the structural predictor for the displacement of the interface Γ at time level $n+1$ contains previous structural information up to time level n only. Thus the general appearance of the scheme is

$$\sum_{i=0}^{n+1} a_i \mathbf{d}_\Gamma^i + \boldsymbol{\mathcal{M}}_{\boldsymbol{\mathcal{A}}} \frac{m^F}{m^S} \sum_{j=0}^{n} b_j \mathbf{d}_\Gamma^j = \mathbf{0}, \tag{54}$$

where $a_i, b_j \in \mathbb{R}$ are the coefficients defining the particular time discretisation scheme. Equation (54) yields the characteristic polynomial

$$p^S(\lambda) + \mu_i \frac{m^F}{m^S} p^F(\lambda) = p(\lambda) = 0, \tag{55}$$

where the polynomial defined by the time discretisation of the structure is denoted by $p^S(\lambda) = \sum_{i=0}^{n+1} a_i \lambda^i$ while the polynomial $p^F(\lambda) = \sum_{j=0}^{n} b_j \lambda^j$ contains the temporal discretisation of the fluid partition, the type of the structural predictor and Dirichlet coupling velocity. The polynomial $p^S(\lambda)$ is one degree higher in λ due to the sequential structure of the problem. Thus we have

$$\frac{p^S(\lambda = -\infty)}{p^F(\lambda = -\infty)} < 0,$$

i.e. both polynomials are of different sign in the infinite negative. As the polynomials are continuous this implies that a point $\lambda^* < -1$ can be found which satisfies

$$\frac{p^S(\lambda^*)}{p^F(\lambda^*)} < 0.$$

Thus there exists a positive coefficient a such that

$$p^S(\lambda^*) + a\, p^F(\lambda^*) = 0.$$

Hence for $a = \max_i \mu_i \frac{m^F}{m^S}$ the characteristic polynomial (55) exhibits a solution with $|\lambda^*| > 1$ and the underlying scheme is thus unstable.

4.4 Discussion of further influences

For a simplified coupled model problem an added mass operator can be defined the eigenvalues of which precisely predict the onset of instabilies[3]. Real fluid structure interaction problems however introduce a significant number of additional influences. There are physical effects which bring more complexity:

- First of all fluid viscosity and structural stiffness cannot be ignored within such applications. Using implicit time discretisation on both fields results in a stabilising

effect of structural stiffness on the added mass instability. Viscous fluid forces however increase the influence of the instability. Clearly both effects depend upon the time step Δt as a reduced time step size decreases the influence of the stiffness terms compared to the mass matrices. Following the results obtained without the influence of the stiffnesses (42) a rough way to get an idea of the stiffness influence is

$$\frac{m^F + a\Delta t k^F}{m^S + b\Delta t^2 k^S} \max_i \mu_i > C_{inst}, \tag{56}$$

where a and b denote constants emerging from the time discretisation while k^F and k^S are characteristic stiffness values representing the positive portion of the stiffnesses. The inequality (56) confirms numerical observations which indicate a stabilising influence of the structural stiffness and a slight destabilising effect of an increased fluid viscosity. If the time step size is decreased the stabilising effect of the structural stiffness decreases faster than the destabilising effect of the fluid viscosity. Thus confirming the destabilising effect of small time step sizes.

- Further there are nonlinearities due to the convective fluid term and also material or geometrical nonlinearities of the structural behaviour. Typically simulations start from a reference configuration and zero velocities and thus the nonlinearities not dominating within the first few steps build up and preclude the existence of a linear added mass operator the eigenvalues of which could predict the stability or instability of a calculation for the entire simulation time.

- Additional nonlinearities also emerge from the geometrical changes due to the displacement of the interface Γ. Changing geometry means changing integration domain and thus a change of all coefficient matrices encountered.

- When compressible structures are employed a change of the effective structural density ρ^S has to be expected which may also influence potential instabilities.

On top of these physical influences the numerical approximation may introduce further difficulties. However numerical studies confirm the theoretical observation and show that the overall behaviour can well be predicted even if a prediction of the precise onset of the instability is almost impossible.

5 NUMERICAL INVESTIGATION

The classical driven cavity problem equipped with a thin flexible bottom is used to numerically investigate the added mass instability within a full fluid structure interaction environment. The example which is taken from Mok[1,2] is depicted in figure 1. The fluid domain is discretised by 32×32 residual based stabilised fluid elements[5,6,7]. We wish to examine the influence of different parameters and discretisation schemes on the onset of

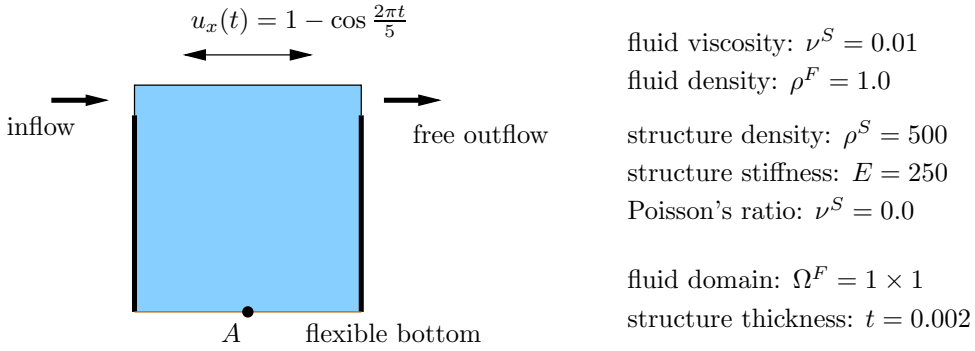

Figure 1: Geometry and material data of driven cavity example with flexible bottom

the instability within the time interval $t \in [0; 100]$. To diagnose stability or instability the history of the vertical component of the FSI coupling force at point A is observed. Oscillations in the coupling force indicate instability. We will call a scheme temporally stable if no such oscillation is observed within the stated time interval of interest.

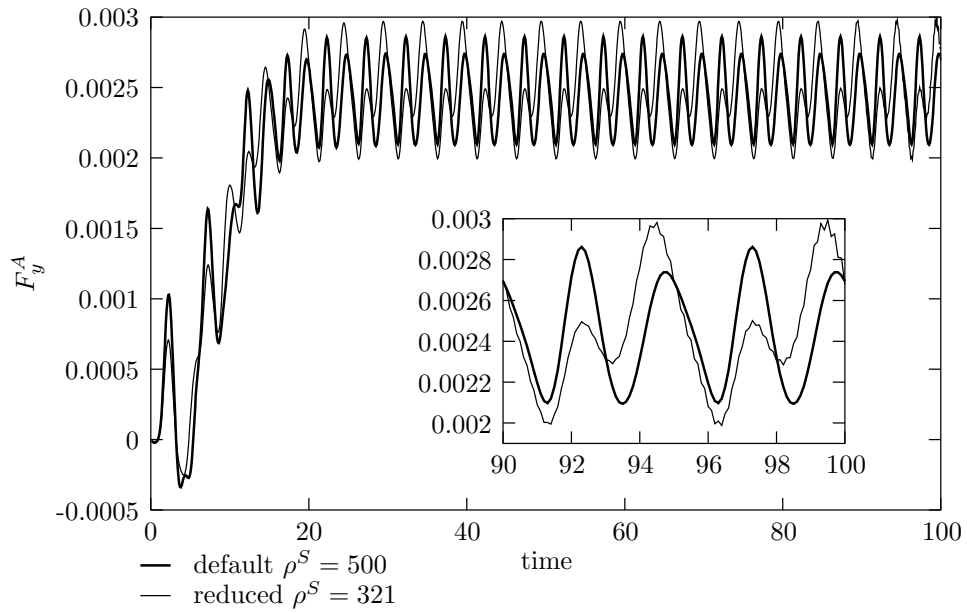

Figure 2: Evolution of the vertical coupling force at point A for the default configuration of parameters and a problem with lower structural mass density both evaluated with BE time discretisation of the fluid

The default algorithm is the most stable scheme to be found. We used generalised-α time integration of the structure with zero spectral radius and BE on the fluid domain.

Further the simple predictor (14) and Dirichlet boundary condition (17) is employed. At a time step of $\Delta t = 0.1$ the problem can stably be integrated in time up to at least 1000 time steps.

The influence of the structural density ρ^S is compared for BE and BDF2 time discretisation on the fluid domain. From the prediction summarised in table 1 we expect that roughly half the structural density required to stably integrate with BDF2 suffices if BE is used on the fluid domain. Starting from the default parameter setting and decreasing the structural density ρ^S the simulation becomes unstable towards the end of the investigated time interval at $\rho^S = 321$. The begin of this instability is depicted in the diagram in figure 2.

A similar procedure is repeated with BDF2 time discretisation on the fluid domain. In this case the problem shows unstable at $\rho^S = 500$ and the structural density is increased until the simulation remains stable within the time interval of interest. Results are shown in the diagram in figure 3. Increasing the structural mass density from $\rho^S = 500$ to

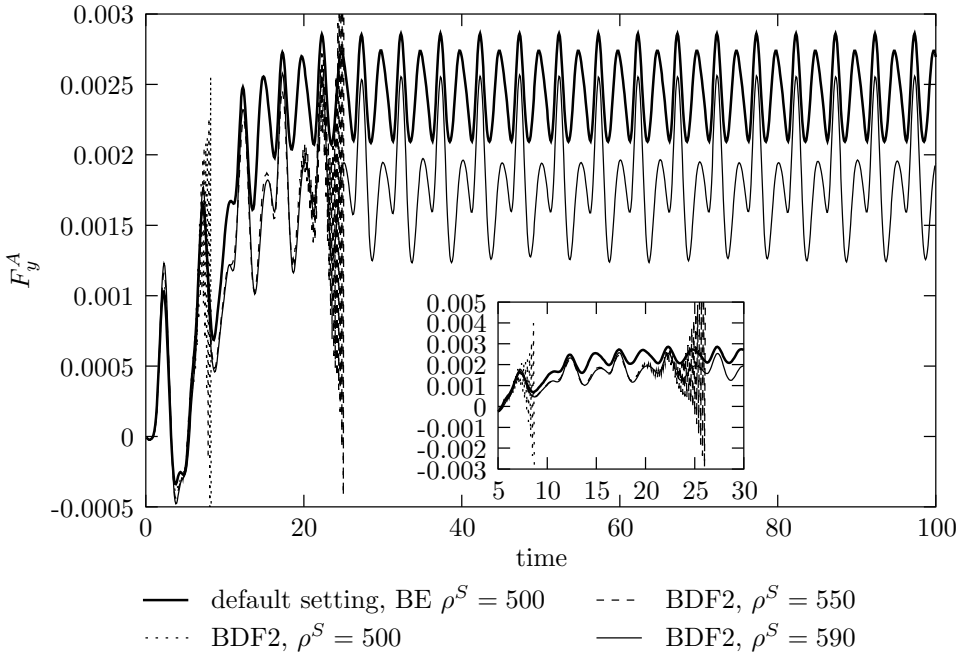

Figure 3: Evolution of the vertical coupling force at point A obtained with the default parameter setting and problems with different structural mass densities obtained with BDF2 time discretisation on the fluid field

$\rho^S = 550$ delays the onset of the instability and also slightly damps the instability itself. At $\rho^S = 590$ no instability is observed within the time interval of interest. This indicates

that within stabilised real FSI applications the instability ratio between BE and BDF2 might be less strict than predicted for the simplified problem as summarised in table 1.

The influence of the structural predictor Further the influence of different structural predictors shall be investigated. Employing the first order accurate predictor (15) rather than (14) yields an immediately unstable scheme at $\rho^S = 500$ even if BE is used to integrate the fluid equations in time. Using the second order accurate predictor (16) the behaviour gets even worse as shown in the diagram 4. From table 1 an estimate of the structural density necessary to stabilise the simulation can be obtained. The zeroth order predictor is stable down to $\rho^S = 322$, thus the first order predictor should be stable for structural densities larger than $\rho^S = 1610$. This prediction fits very well as the first stable simulation with the first order predictor is obtained at $\rho^S = 1635$. Similar observations can be made when the second order accurate predictor is used which yields an instability condition nine times as rigorous as the zeroth order one. Thus the smallest structural density which should allow for a stable computation is $\rho^S = 2898$. Actually at $\rho^S = 2300$ no oscillations are observed within the time interval of interest while in this case it starts to oscillate within the next few steps.

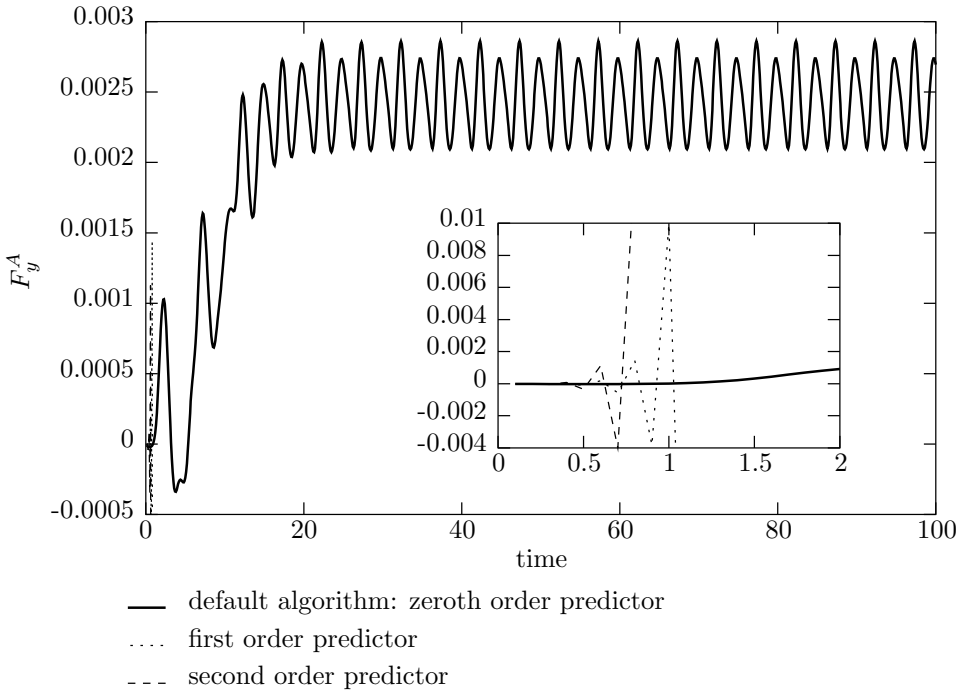

Figure 4: Evolution of the vertical coupling force at point A evaluated with default parameter setting and different predictors: within the first few time steps violent instabilities are observed if higher order predictors are employed

6 CONCLUSIONS

The destabilising added mass effect in the context of fluid structure interaction computations is not an artifact of a particular discretisation scheme. It rather is an inherent property of sequentially staggered scheme itself and cannot be decreased by increasing the accuracy. Nevertheless there are time discretisation schemes for the fluid equations which allow for a stable calculation at high ratios between structural and fluid density. Such schemes which exhibit stationary characteristics of the respective time discretisation schemes yield an instability condition of the form

$$\frac{m^F}{m^S} \max_i \mu_i > C$$

indicating instability when satisfied. It turns out that the constant C is the smaller the higher the temporal accuracy of the scheme. Thus stability and high accuracy cannot be achieved at the same time when sequentially staggered schemes are employed.

Schemes with recursive characteristics yield an instability condition of the form

$$\frac{m^F}{m^S} \max_i \mu_i > \frac{C}{n}$$

and will thus definitely become unstable for every density ratio if the simulation time is long enough. While 'long enough' is usually reached rather soon. Among the schemes considered here the trapezoidal rule (and more generally the implicit one-step-θ method for all $\theta < 1$) yield such necessarily unstable schemes. But also the use of the correct second order boundary condition along the interface Γ (18) results in a scheme with recursive characteristics which is thus unstable after a small number of steps.

The artificial added mass effect imposes a lower bound on the time step for schemes which allow for conditionally stable computations. An upper bound on the time step results from the CFL condition introduced by the explicit character of the sequential coupling. Thus for practical applications the range of allowed time step sizes might be rather small or even empty due to an overlap of both restrictions.

There is further a limit density ratio for every scheme irrespective of the actual representation of the added mass operator which provides an ultimate instability condition. Thus no sequentially staggered scheme can be constructed which would be unconditionally stable with respect to the density ratio.

In the case that residual based stabilisation is employed on the fluid field the discrete representation of the added mass operator and thus its eigenvalues are influenced by stabilisation terms. Consequently further effects can be observed[5].

The actual parameters at which the instability will occur are hard to predict precisely especially when significant nonlinearities have to be considered. However the relationship between different time discretisation schemes with respect to their influence on the instability provides some information which applies also to real FSI calculations. Numerical

investigations further indicate that for FSI calculations coupling slender structures with incompressible flow the density ratio at which stable simulations can be performed is very restrictive. Thus the conclusion drawn by Mok[1,2] is justified; iteratively staggered schemes are to be preferred within most such FSI calculations.

7 ACKNOWLEDGEMENT

The present study is supported by a grant of the foundation "Deutsche Forschungsgemeinschaft" (DFG) under project B4 of the collaborative research centre SFB 404 'Multifield Problems in Continuum Mechanics'. This support is gratefully acknowledged.

REFERENCES

[1] D.P. Mok and W.A. Wall. Partitioned analysis schemes for the transient interaction of incompressible flows and nonlinear flexible structures. In: *Proceedings of Trends in Computational Structural Mechanics*, W.A. Wall, K.-U. Bletzinger and K. Schweitzerhof (Eds.), (2001).

[2] W.A. Wall, D.P. Mok and E. Ramm. Partitioned analysis approach of the transient coupled response of viscous fluids and flexible structures. In: *Solids, Structures and Coupled Problems in Engineering, Proceedings of the European Conference on Computational Mechanics ECCM '99, Munich*, W. Wunderlich (Ed.), (1999).

[3] P. Causin, J.-F.Gerbeau and F. Nobile. Added-mass effect in the design of partitioned algorithms for fluid-structure problems. *Comp. Meth. Appl. Mech. Engrg.*, **194**, 4506–4527, (2005).

[4] J. Chung and G.M. Hulbert. A time integration algorithm for structural dynamics with improved numerical dissipation; The Generalized-α method. *J. Appl. Math.*, **60**, 371–375, (1993).

[5] Ch. Förster, W.A. Wall and E. Ramm. Artificial added mass instabilities in sequential staggered coupling of nonlinear structures and incompressible viscous flows. *submitted to Comp. Meth. Appl. Mech. Engrg.*, (2006).

[6] L.P. Franca and C. Farhat. Bubble functions prompt unusual stabilized finite element methods. *Comp. Meth. Appl. Mech. Engrg.*, **123**, 299–308, (1995).

[7] L.P. Franca and F. Valentin. On an improved unusual stabilized finite element method for the advective-reactive-diffusive equation. *Comp. Meth. Appl. Mech. Engrg.*, **190**, 1785–1800, (2000).